ELSEVIER

Contents lists available at ScienceDirect

Computer Physics Communications

journal homepage: www.elsevier.com/locate/cpc



Computer Programs in Physics



Photoionization cross sections and photoelectron angular distributions of molecules with XCHEM-2.0 $^{\cancel{\bowtie}, \cancel{\bowtie} \cancel{\bowtie}}$

Vicent J. Borràs ^a, Pedro Fernández-Milán ^a, Luca Argenti ^b, Jesús González-Vázquez ^{a,c,*}, Fernando Martín ^{a,d,e,**}

- ^a Departamento de Química, Módulo 13, Universidad Autónoma de Madrid, 28049 Madrid, Spain
- b Department of Physics and CREOL, University of Central Florida, Orlando, FL 32186, USA
- c Institute for Advanced Research in Chemical Sciences (IAdChem), Universidad Autónoma de Madrid, 28049 Madrid, Spain
- d Instituto Madrileño de Estudios Avanzados en Nanociencia (IMDEA Nano), Cantoblanco 28049 Madrid, Spain
- ^e Condensed Matter Physics Center (IFIMAC), Universidad Autónoma de Madrid, 28049 Madrid, Spain

ARTICLE INFO

Keywords:

Molecular photoionization

Feshbach resonances

Molecular-frame photoelectron angular distri-

butions

Asymmetry parameters

ABSTRACT

The XCHEM code was introduced in 2017 [1] to provide an accurate description of electron correlation and exchange in the electronic continuum of molecules at the same level as complete or restricted active-space self-consistent field (CASSCF or RASSCF) methods. This has allowed for an accurate description of molecular photoionization in the region of Feshbach resonances, shake up processes in which ionization is accompanied by excitation of one or several of the remaining electrons, and interchannel couplings. The success of XCHEM for small molecules has led us to improve its performance in several aspects, which now allows for the description of resonant molecular photoionization in larger systems. In addition, we have incorporated the possibility to calculate photoelectron angular distributions in the laboratory and molecular frames, which are essential to interpret angularly resolved photoionization experiments. Here we show its performance in the N₂ and pyrazine molecules. The new version of the code, XCHEM-2.0, is freely available at https://gitlab.com/xchem/xchem_public.

Program summary

Program Title: XCHEM-2.0

CPC Library link to program files: https://doi.org/10.17632/t8tbk9gdt2.1

Developer's repository link: https://gitlab.com/xchem/xchem_public/-/archive/2.0.0/xchem_public-2.0.0.tar.gz

Licensing provisions: LGPL

Programming language: Fortran, python

Nature of problem: Understanding photoionization of molecules is a recurrent goal in Atomic, Molecular and Optical physics, even more nowadays with the advent of XUV and X-ray high-harmonic generation sources and free electron lasers. Photoionization can be employed to induce electron dynamics in molecules, e.g., by using ultrashort XUV or X-ray pulses, or as a probe of these dynamics by recording time-resolved photoelectron spectra. At low photoelectron energies, photoionization may result from various competing processes, such as direct ionization, autoionization of Feshbach and shape resonances, shake up, etc., each of these leaving its trace in the measured spectra. So, interpretation of these spectra can be a difficult task and theoretical simulations are often required to separate the different contributions. However, a method able to do so must be able to describe electron correlation in the electronic continuum beyond the Hartree-Fock (HF) and configuration interaction singles (CIS) approximations. XCHEM-2.0 has been designed to account for all these processes by providing an accurate description of electron correlation in the ionization continuum of molecules.

https://doi.org/10.1016/j.cpc.2023.109033

Received 21 June 2023; Received in revised form 23 November 2023; Accepted 24 November 2023

 $^{^{*}}$ The review of this paper was arranged by Prof. Jimena Gorfinkiel.

[†] This paper and its associated computer program are available via the Computer Physics Communications homepage on ScienceDirect (http://www.sciencedirect.com/science/journal/00104655).

^{*} Corresponding author at: Institute for Advanced Research in Chemical Sciences (IAdChem), Universidad Autónoma de Madrid, 28049 Madrid, Spain.

^{**} Corresponding author at: Departamento de Química, Módulo 13, Universidad Autónoma de Madrid, 28049 Madrid, Spain. E-mail addresses: jesus.gonzalezv@uam.es (J. González-Vázquez), fernando.martin@uam.es (F. Martín).

Solution method: XCHEM-2.0 employs a close coupling formalism to describe the electronic continuum of molecules at the level of multiference configuration interaction (MRCI) methods in combination with a hybrid Gaussian-Bspline basis set (the so-called GABs basis). In particular, it makes use of a restricted active space self-consistent field (RASSCF) approximation to evaluate the bound electronic states of the remaining molecular cation using localized Gaussian functions. These localized Gaussians are then supplemented with a single centered Gaussian expansion to allow the electron to leave the nuclear environment. Finally, the basis set includes a set of B-spline functions, centered at the same position as the single-centered Gaussians, which reach the asymptotic region. Thanks to the last B-spline function, which does not vanish at the box boundary, XCHEM-2.0 can determine continuum states fulfilling any required asymptotic behavior. The present version of the code improves on the original version by incorporating a more efficient augmentation procedure to build N_e -electron configurations from (N_e – 1) ones, reducing the space to store data, providing a more efficient removal of linear dependencies resulting from the over-completeness of the polycentric+GABS basis and a more efficient solution of the scattering equations, and including new routines to calculate photoelectron angular distributions in the laboratory and molecular frames.

Additional comments including restrictions and unusual features: The proposed method focuses on RASSCF methodology, so part of electron correlation is still not included. Also, one- and two electron integrals involving exclusively Gaussian functions are done using a modified version of the OpenMOLCAS software, so the installation of this code is also required and limitation associated with the latter is applicable. The code is limited to include a few ionization channels (around 20) with medium angular momentum (limited to $\ell=15$ as in OpenMOLCAS).

1. Introduction

The development of theoretical methods aiming at describing molecular photoionization has received an important push since the beginning of the 21st century. Two major experimental developments have spurred researchers to go in this direction: the advent of attosecond light pulses through the process of high harmonic generation (HHG) [2-9] and the recent production of few-femtosecond or even subfemtosecond light pulses in large-scale free electron laser (FEL) facilities [10-13]. In both cases, the generated pulses lie in the extreme ultraviolet (XUV) and soft X-ray regions, so that any atom, molecule, or material can be ionized by absorbing just a single photon. And this occurs in a gentle way, i.e., without appreciably affecting the potential that holds the electrons in the target, despite the high intensities provided by FELs, due to the high frequency of the light associated with these pulses (Keldysh parameter much larger than one). This means that the interaction can be well described by a truncated perturbative expansion. A good starting point for the theoretical descriptions of the photoionization process is, therefore, the evaluation of the electronic continuum states of the system in the absence of the radiation field.

The advent of synchrotron radiation sources in the late 20th century has promoted the development of several codes to model the ionization processes of atomic systems with varying levels of approximation (see e.g., [14-18]). However, the number of codes able to describe the ionization of molecules is appreciably smaller. This is mostly due to the multicenter character of both bound and continuum electronic wave functions, and the well-known slow convergence of electron correlation in molecular system with respect to the size of the configurationinteraction space needed to reproduce it. The latter limitation is particularly challenging in the electronic continuum due to the presence of Feshbach resonances and the fact that, in contrast to atomic systems, the number of accessible partial waves is in principle infinite due to the lack of angular selection rules. For this reason, some of the existing molecular codes are designed to describe ionization in regions where Feshbach resonances are absent, or ignore all or some interchannel couplings, or consider regions of the spectra far from the ionization threshold, where the ejected electrons are too fast to appreciably interact with the remaining electrons [3,19,20]. Some other codes are designed to minimize as much as possible the multi-center character of the electronic continuum [21,22] and, therefore, are appropriate to describe the ionization continuum at very high electron energy.

Many current experiments performed with XUV pulses in molecules, however, lead to photoelectrons in a region within few tens of eV from the ionization threshold (see, e.g., [23–28]). In this region of the ionization continuum we often find several states of the molecular ion,

corresponding to several excitation thresholds. Each threshold is associated, on the one side, to multiple Rydberg series of Feshbach resonances and, on the other side, to shake up processes in which ionization is accompanied by excitation of one or several of the remaining electrons, for which interchannel couplings cannot be ignored. Therefore, fully correlated methodologies must be used, as e.g., the complex Kohn method [29-33], the multichannel Schwinger configuration interaction approach (MCSCI) [34-37], the UK Molecular R-Matrix method (UK-MolRM) [38], tRecX [39], ASTRA [40] and the XCHEM method [1]. A common characteristic of all of them is that they combine existing multireference quantum chemistry packages, e.g., OpenMolcas [41], MOLPRO [42], GAMESS [43], DALTON [44], or LUCIA [45], specially designed to deal with the multicenter character of the molecular potential and to accurately describe electron correlation in bound states, with scattering theory methods appropriate to describe the ionization continuum. Quantum chemistry methods make use of Gaussian basis functions centered on the atomic nuclei, which allow for an efficient and accurate evaluation of two-electron integrals involving several centers. However, Gaussian functions decrease exponentially at long distances, so that they are not appropriate to describe the asymptotic oscillating behavior of continuum wave functions [46]. For this reason, in addition to combining the available quantum chemistry packages with the necessary scattering tools, additional basis functions able to describe the continuum wave functions in the asymptotic region are necessary. This can be done by supplementing the Gaussian basis with a finite-element (FE) [47,48] or a discrete variable representation (DVR) [49-51] of the radial coordinate, with plane waves [52], or B-spline functions [53,54].

The XCHEM code [1] was originally designed to provide an accurate description of electron correlation and exchange in the electronic continuum of molecules at the same level as complete or restricted active-space self-consistent field (CASSCF or RASSCF) methods [55]. Therefore, it is ideal to describe Feshbach resonances in the electronic continuum, shake up processes and interchannel couplings. XCHEM makes use of a hybrid Gaussian-B-spline basis (GABS) [46] to supplement the polycentric Gaussian basis functions provided by Quantum Chemistry packages. The GABS consists of a large number of monocentric Gaussian and B-spline functions, all placed at the center of mass of the molecule (although they can be placed elsewhere if desired), with the B-spline functions starting at a given radius R_0 and going as far away as desired. A clever choice of R_0 allows one to avoid evaluating expensive one- and two-electron integrals that simultaneously involve polycentric Gaussian and the B-spline functions. These integrals can only be performed numerically. All the remaining integrals are evaluated analytically, which is very convenient when calculations involve a large number of electronic configurations. XCHEM leverages the B-

spline flexibility to determine, within a close-coupling approach [56]. the molecular electronic scattering states that fulfill required boundary conditions, thus providing the necessary dipole transition matrix elements (bound-bound, bound-continuum and continuum-continuum) to evaluate the ionization probabilities, cross sections, and photoelectron distributions in the framework of perturbation theory, for one-photon transitions [57-61], or by solving the time-dependent Schrödinger equation (TDSE), for multi-photon ionization processes [62-64]. Although evaluation of these couplings is limited to the box part of the wave function, this has been shown to be an excellent approximation to evaluate one-photon ionization cross sections in atoms [1,65,62,63] and molecules [1,57-61], and to simulate one-photon and multiphoton above-threshold ionization by ultrashort pulses, provided that all couplings, in particular continuum-continuum ones, are consistently evaluated in the same box and the photoelectron wave packet remains confined to the quantization box while the external field is on (see, e.g., [64]). Physically, this means that the photoelectron does not have the time to reach the box boundaries. In particular, once the light field is over, the projection of the wave packet on the scattering states of the field free Hamiltonian yields a photoelectron distribution that is time invariant, and hence exact.

In order to go to larger molecules while preserving the computational advantages of XCHEM, in the last few years we have increased the computational efficiency of several of its routines by adopting new algorithms. These improvements mainly affect (i) the augmentation procedures used to build N_e -electron configurations from (N_e-1) ones, i.e., to build the N_e -electron wave functions from the (N_e-1) states of the cation, (ii) the way data are stored (now, using the HDF5 library [66]), (iii) a more efficient removal of linear dependencies resulting from the overcompleteness of the polycentric+GABS basis and (iv) a more efficient solution of the scattering equations. In addition, (v) we have included new routines that provide photoelectron angular distributions [60] in the laboratory and molecular frames, which are essential to interpret angularly resolved experiments. The new version of the code, XCHEM-2.0, is available at https://doi.org/10.17632/t8tbk9gdt2.1.

In this paper, we describe the most formal aspects of these improvements, with a focus on the augmentation procedure and the solution of the scattering equations. The performance of the new XCHEM-2.0 release is illustrated by calculations of photoionization cross sections and photoelectron angular distributions in the lab and molecular frames for N₂ and pyrazine. For N₂, comparison with available experimental data is provided. For pyrazine, our results are predictions that should be confirmed in future experiments. In both cases, the presence at low energies of Feshbach resonances corresponding to diffuse Rydberg states associated with the different ionization thresholds introduces radical changes in the electron angular distributions. Although these variations may be experimentally invisible in the case of very narrow (i.e., long lived) resonances, due to nuclear motion or insufficient energy resolution, those associated with the broader resonances should be observable. This should be the case of the Hopfield series of resonances in N2 and of the lowest Feshbach resonances in pyrazine.

The paper is organized as follows. In Section 2, we describe the general theoretical framework and the formal aspects of the improved augmentation procedure, the new method to solve the scattering equations to impose the appropriate boundary conditions and the basic equations used in our implementation of electron angular distributions. In section 3, we present our results for $\rm N_2$ and pyrazine, and in section 4 the main conclusions of the present work. Atomic units are used throughout unless otherwise stated.

2. XCHEM approach

The theory behind the XCHEM approach has been described in detail in Ref. [1], so here we will only summarize its basic ingredients in 2.1 and we will concentrate in the rest of the section on the new features available in the present version of the code.

2.1. General framework

The N_e -electron wave function $\Psi_{\alpha E}$ describing a molecular cation with N_e-1 electrons and an electron in the ionization continuum of the neutral molecule is written as the close-coupling expansion

$$\begin{split} \Psi_{\alpha E}(\{\mathbf{x}\}_{N_e}) &= \sum_i c_{i,\alpha E} \aleph_i(\{\mathbf{x}\}_{N_e}) \\ &+ \sum_{\beta i} \left[N_{\beta i} \hat{\mathcal{A}} \Upsilon_{\beta}(\{\mathbf{x}\}_I; \hat{r}_{N_e}, \zeta_{N_e}) \phi_i(r_{N_e}) \right] c_{\beta i,\alpha E}, \end{split} \tag{1}$$

where \aleph_i denotes short range states with all electrons occupying bound orbitals φ_{QC} , $\phi_i(r_{N_e})$ denotes the radial component of the electron ejected to the continuum, and Υ_β is a channel function. The notation $\{\mathbf{x}\}_{N_e/I}$ indicates all or all but one (the photoelectron's) electronic coordinates, respectively. A channel function Υ_β with total spin S and spin projection Σ is represented by an ionic molecular state Φ_b (with spin S_b and spin projection Σ_b) coupled to an electron with orbital angular momentum quantum numbers l and m

$$\begin{split} \Upsilon_{\beta}(\{\mathbf{x}\}_{I}) &= {}^{2S+1} \left[\Phi_{b}(\{\mathbf{x}\}_{I}) \otimes \chi(\zeta_{N_{e}}) \right]_{\Sigma} X_{lm}(\hat{r}_{N_{e}}) \\ &= \sum_{\Sigma_{b}\sigma} C_{S_{b}\Sigma_{b}, \frac{1}{2}\sigma}^{S\Sigma} {}^{2S_{b}+1} \Phi_{b,\Sigma_{b}} {}^{2} \chi_{\sigma} X_{lm} , \end{split} \tag{2}$$

where $C_{S_b\Sigma_b,\frac{1}{2}\sigma}^{S\Sigma}$ are Clebsch-Gordon coefficients, X_{lm} are symmetryadapted spherical harmonics, and χ is the spin component of the photoelectron. In Eq. (1), all terms but $\phi_i(r_{N_e})$ decrease exponentially and vanish far from the center of mass of the molecule, so that they can be evaluated by using multi-reference quantum chemistry methods with polycentric Gaussian (PCG) basis functions centered on the atomic positions. To represent the asymptotic oscillatory behavior of $\phi_i(r_{N_a})$, we use a hybrid basis of Gaussian and B-spline functions, GABS, which includes monocentric gaussian (MCG) functions, $G^{M}(r)$, that effectively extend up to a radius R_1 , and B-spline functions defined in a linear grid beyond a radius R_0 . This radius should be large enough to ensure negligible overlap between B-splines and PCG functions, but small enough to ensure a significant overlap with the MCG functions. The antisymmetrized products in the second line of equation (1), also called the extended-channel functions $\bar{\Upsilon}_{\alpha i}(\{\mathbf{x}_N\})$, are constructed by augmenting the ionic states Φ_b with an electron in an orbital built from either of the above mentioned basis functions. In this way, in the region where $r < R_0$, the full wave function is exclusively expressed in terms of PCGs and MCGs, which allows us to compute matrix elements using standard methods implemented in quantum chemistry packages. More interestingly, matrix elements that involve both the parts of the wave function exclusively represented by PCGs (the inner part) and those parts resulting from the augmentation of a given channel functions with a B-spline (the outer part) can be neglected [46]. In other words, if the radius R_0 is chosen such that the values of the PCGs do not exceed a given threshold, say 10^{-8} , their overlap with the B-splines, which are only defined for $r > R_0$, will be nearly zero, so that any integral involving both kinds

2.2. Augmentations

We use multiconfigurational methods to obtain the parent ion wave function Φ_a . Specifically, we use the restricted active space self consistent field approximation [55]. In this way, the parent ion wave functions are expressed as linear combinations of configuration state functions (CSF) with a well-defined spin:

of functions can safely be neglected, including two-electron integrals.

$$\Phi_a(\mathbf{x}) = \sum c_{ia}{}^M \Xi_i(\mathbf{x}),\tag{3}$$

where $\Phi_a(\mathbf{x})$ is an (N_e-1) -electron parent-ion wave function with multiplicity M. Once the parent ions are defined, we need to include an extra electron that eventually can be ejected to the continuum. This is

done by augmenting the different parent ions in every possible orbital. To do this augmentation, we convert the wave function from CSFs (Ξ) to Slater Determinants (D_i) . In our case, we extract the GUGA table from the OpenMOLCAS package [41], obtaining the parent ion wave functions as:

$$\Phi_a(\mathbf{x}) = \sum_i c'_{ia} D_i(\mathbf{x}) \tag{4}$$

The Slater determinants are constructed with orbitals ϕ_i^L that result from the linear combinations of Gaussian basis functions localized at the atomic sites, hence the superscript L

$$\phi_i^L(\mathbf{x}_1) = \sum_i d_{ii} G_j^L(\mathbf{x}_1). \tag{5}$$

In our approach all the parent ions must be described with the same set of orbitals. One option is to use the state-averaged formalism, SA-CASSCF, where the orbitals are optimized for an hypothetical wave function containing all states of interest. After evaluation of the different parent ions, the non-occupied orbitals are removed from the system and the MCG functions belonging to the GABs basis [46] are incorporated. Finally, the parent ions are augmented with an extra electron in all possible orbitals, i.e. localized and monocentric orbitals:

$$\bar{\Phi}_{ai}(\mathbf{x}) = a_i^{\dagger} \Phi_a(\mathbf{x}), \tag{6}$$

where $\bar{\Phi}_{ai}$ represents the parent ion a augmented with an electron in orbital i. Since our parent ion wave function is given by Slater determinants, (see equation (4))

$$\bar{\Phi}_{ai}(\mathbf{x}) = \sum_{j} c'_{ja} a_i^{\dagger} D_j(\mathbf{x}) = \sum_{j} c''_{ja} D'_j(\mathbf{x})$$
 (7)

where D'_{j} is the augmented Slater determinant. Finally, the augmented wave function is projected back to CSFs with the neutral GUGA table:

$$\bar{\Phi}_{ai}(\mathbf{x}) = \sum_{j} a_{ji}{}^{M'} \Xi_{j}(\mathbf{x}) \tag{8}$$

where M' = 2S + 1 refers to the multiplicity of the augmented parent ion, as depicted in Eq. (1). Once the augmented wave functions are obtained as combination of CSFs, the different electronic matrix elements are obtained. Specifically, Hamiltonian, overlap and dipole matrix elements are evaluated in the basis of the augmented states. After that, B-splines functions belonging to the GABS basis are added and the corresponding matrix elements are evaluated as described in Ref. [1].

Finally, in the original work, the coupling matrix elements were calculated using the RASSI program of the OpenMolcas [41] package when only Gaussian functions were involved. However, in the case of two-electron integrals, calculations with OpenMolcas can become prohibitively expensive when increasing the angular momentum (since more monocentric basis functions must be added to the calculation). In the present version of XCHEM, this is solved by using a two-exponent scheme, where OpenMolcas only has two-exponents of the monocentric basis and they are combined afterwards. In this way, OpenMolcas never sees the full monocentric basis set but only a reduced set, thus decreasing the computational requirements.

2.3. Evaluation of continuum states with proper boundary conditions

At variance with the original version of XCHEM [1], in this version of the code the continuum states or scattering states are evaluated following the procedure introduced by Harkema et al. for atomic photoionization [67]. In this new implementation, the scattering states are stored in a linked list, which allows using different options to set and improve the energy grid, offering more flexibility and in general a very good performance.

The scattering states must fulfill incoming boundary conditions

$$\Psi_{\alpha E}^{-} \xrightarrow[r_{N_e} \to \infty]{} \frac{1}{N_e} \sum_{\beta} \Upsilon_{\beta} \frac{u_{\beta, \alpha E}^{-}(r_{N_e})}{r_{N_e}}, \tag{9}$$

where

$$u_{\beta,\alpha E}^{-} = \delta_{\alpha\beta} \sqrt{\frac{2}{\pi k_{\alpha}}} e^{i\Theta_{\alpha}(r_{N_e})} + \sqrt{\frac{2}{\pi k_{\beta}}} e^{-i\Theta_{\beta}(r_{N_e})} S_{\beta\alpha}^{\star}, \tag{10}$$

S denotes the scattering matrix, and $\Theta_{\alpha}(r) = k_{\alpha}r + \frac{Z}{k_{\alpha}}\ln 2k_{\alpha}r - l_{\alpha}\pi/2 + \sigma_{l_{\alpha}}(k_{\alpha})$, where k_{α} , Z and $\sigma_{l_{\alpha}}$ are the magnitude of the momentum of the ejected electron, the charge of the parent ion and the Coulomb phase, respectively [68].

To avoid undesired linear dependencies due to over-completeness of the basis that includes both polycentric and monocentric Gaussian functions, we first diagonalize the overlap matrix in this combined basis. From the resulting eigenvectors, we then remove those associated to eigenvalues smaller than a selected threshold (usually of the order of 10^{-8}). Hence, a new linearly independent and orthonormal basis is created. This basis is then employed to create a set of orthonormal orbitals that do not overlap with the orbitals previously obtained with polycentric gaussians (including those in both active and inactive spaces). Then we diagonalize the Hamiltonian in the basis built by augmenting the parent-ion wave functions with both the new linearly independent gaussian basis and the B-splines. This leads to a discrete spectrum instead to a continuous one. However, scattering states must fulfill the Scrhödinger equation for arbitrary values of the energy E. For this, the coefficients of the last B-splines placed at the end of the box ($|B_{\alpha}^{last}\rangle$), which are set to zero to obtain the box states, must in general be different from zero. Thus, we write the scattering states as a linear combination of the box eigenstates ($|\Phi\rangle$) plus the parent ions augmented with the last B-splines ($|B_{\alpha}^{last}\rangle$),

$$\left|\Psi_{\beta E}\right\rangle = \sum_{i=1}^{N} \left|\Phi_{i}\right\rangle c_{i} + \sum_{\alpha=1}^{M} \left|B_{\alpha}^{last}\right\rangle c_{\alpha}^{\beta},\tag{11}$$

where N is the total number of box states, M is the number of open channels at the energy E, and β refers to one of the different M open channels. By requiring that the scattering states $\left|\Psi_{\beta E}\right\rangle$ satisfy the Schrödinger equation $\left[\left(E-H\right)\left|\Psi_{\beta E}\right\rangle=0\right]$ within the box-eigenstate space and multiplying by $\left\langle\Phi_{j}\right|$, we obtain the following expression for the expansion coefficients c_{j}

$$c_{j} = \sum_{\alpha=1}^{M} \frac{E \left\langle \Phi_{j} \left| B_{\alpha}^{last} \right\rangle - \left\langle \Phi_{j} \middle| \widehat{H} \left| B_{\alpha}^{last} \right\rangle \right.}{E_{j} - E} c_{\alpha}^{\beta}$$

$$(12)$$

Given a set of coefficients c_{α}^{β} defining the value of $\Psi_{\beta E}$ at the box boundaries, the number of linearly independent solutions for the $\{c_j\}$ coefficients at the energy E is equal to the number of open channels. When the energy E does not coincide with or is not close to any box eigenvalue E_j , we choose $c_{\alpha}^{\beta}=\delta_{\alpha\beta}$ for all open channels, so that the corresponding scattering function has the following expression

$$|\Psi_{\alpha E}\rangle = \sum_{i=1}^{N} |\Phi_{i}\rangle \frac{\langle \Phi_{i} | (E - \hat{H}) | B_{\alpha}^{last} \rangle}{E_{i} - E} + |B_{\alpha}^{last} \rangle. \tag{13}$$

This formula may fail if E is extremely close to one of the box eigenvalues E_j , since the corresponding box eigenstate would be represented with a coefficient much larger than all the others. In other terms, as E approaches E_j , all the scattering states generated with this formula, once normalized, approach the box eigenstate $|\Phi_j\rangle$. As a consequence, when reconstructing the set of orthogonal scattering states, a cancellation error may emerge. For most practical purposes, it is unlikely for the sampled energy to fall within a distance from a box eigenstate energy so small (e.g., 10^{-10} a.u.) that such a cancellation error would be

of any concern. In principle, however, this possibility should be taken into account.

To determine how to do so, we first consider the limiting case of $E=E_j$ exactly. At $E=E_j$, the state $|\Phi_j\rangle$ is already an exact scattering state, namely, that one state that happens to vanish at the box boundary in all channels. Indeed, it is this specific boundary requirement that causes the energy of the confined system to be quantized. All the other states can be obtained by selecting the boundary conditions c_α^β for the residual M-1 channels ($\alpha=1,2,...,M-1$) in the M-1 dimensional space of vectors orthogonal to the boundary coupling vector $\langle \Phi_j | (E-\hat{H}) | B_\alpha^{last} \rangle$, e.g., by means of a Gram-Schmidt orthonormalization to this initial vector. In these cases, the coefficient c_j of the solution in the box can be chosen to be zero, thus eliminating any potential issue at its root.

This consideration can guide the design of the algorithm also when E is very close to, but distinct from E_j . While $|\Phi_j\rangle$ is not a legitimate scattering state in this case, it can be expected that it will be very close to one of the required scattering states, with minor contributions from the other box states and the boundary functions, particularly those most strongly coupled with $|\Phi_j\rangle$. A possible approach starts from identifying a boundary state γ that is maximally coupled with $|\Phi_j\rangle$, $\forall \alpha$, $|\langle \Phi_j|(E-\hat{H})|B_{\alpha}^{last}\rangle| \geq |\langle \Phi_j|(E-\hat{H})|B_{\alpha}^{last}\rangle|$. The scattering state closest to $|\Phi_j\rangle$, say $|\Psi_{\gamma E}\rangle$, can then be determined by imposing $c_{\gamma}^{\beta} = -\delta_{\beta\gamma}(E-E_j)$, so that

$$\begin{split} |\Psi_{\gamma E}\rangle = &|\Phi_{j}\rangle\langle\Phi_{j}|(E-\hat{H})|B_{\gamma}^{last}\rangle \\ &-\left[\sum_{i\neq j}|\Phi_{i}\rangle\frac{\langle\Phi_{i}|(E-\hat{H})|B_{\gamma}^{last}\rangle}{E_{i}-E} - |B_{\gamma}^{last}\rangle\right](E-E_{j}). \end{split} \tag{14}$$

As in the previous case, the remaining M-1 solutions can be determined by setting $c_j=0$ and choosing boundary conditions compatible with this choice, i.e., with boundary coefficients c_α^β that are orthogonal to the boundary-coupling vector to the $|\Phi_j\rangle$ box eigenstate, $\langle \Phi_i | (E-\hat{H}) | B_\alpha^{last} \rangle$,

$$|\Psi_{\beta \neq \gamma E}\rangle = \sum_{i \neq j} |\Phi_i\rangle \sum_{\alpha=1}^{M} \frac{\langle \Phi_i | (E - \hat{H}) | B_{\alpha}^{last} \rangle c_{\alpha}^{\beta}}{E_i - E} + \sum_{\alpha} |B_{\alpha}^{last} \rangle c_{\alpha}^{\beta}. \tag{15}$$

The M different degenerate solutions $|\Psi_{\alpha,E}\rangle$ will serve as a basis to construct the scattering states satisfying the correct boundary conditions. For large values of the radial coordinate of any of the electrons in the system, say, $r_{N_e} \to \infty$, $\Psi_{\alpha,E}$ must behave as a linear combination of the regular $\mathcal F$ and irregular $\mathcal G$ Coulomb functions in each of the M open channels in the close-coupling expansion

$$\Psi_{\alpha,E} \xrightarrow[N_e \to \infty]{} \frac{1}{N_e} \sum_{\beta}^{\text{open}} \Upsilon_{\beta} \frac{u_{\beta,\alpha E}(r_{N_e})}{r_{N_e}}$$
 (16)

where

$$u_{\beta,\alpha E}(r_{N_{\alpha}}) = A_{\beta\alpha} \mathcal{F}_{\beta}(r) + B_{\beta\alpha} \mathcal{G}_{\beta}(r), \tag{17}$$

and, for simplicity, we have used the notation $\mathcal{F}_\beta(r)=\sqrt{\frac{8}{\pi k_\beta}}\mathcal{F}(k_\beta r)$

and $\mathcal{G}_{\beta}(r)=\sqrt{\frac{8}{\pi k_{\beta}}}\mathcal{G}(k_{\beta}r)$. The values of the Coulomb functions at the end of the box, $\mathcal{F}_{\beta}(R_{max})$ and $\mathcal{G}_{\beta}(R_{max})$, and their first derivatives, $\mathcal{F}'_{\beta}(R_{max})$ and $\mathcal{G}'_{\beta}(R_{max})$, are known. From the value of the $u_{\beta,\alpha E}(R_{max})$ and $u'_{\beta,\alpha E}(R_{max})$, therefore, we can readily determine the values of $A_{\beta,\alpha E}$ and $B_{\beta,\alpha E}$ by solving the following linear system of 2M equations.

$$\begin{cases} \mathcal{F}_{\beta}(R_{max})A_{\beta,\alpha E} + \mathcal{G}_{\beta}(R_{max})B_{\beta,\alpha E} = u_{\beta,\alpha E}(R_{max}) \\ \mathcal{F}'_{\beta}(R_{max})A_{\beta,\alpha E} + \mathcal{G}'_{\beta}(R_{max})B_{\beta,\alpha E} = u'_{\beta,\alpha E}(R_{max}). \end{cases}$$
(18)

Since, asymptotically,

$$\sqrt{\frac{2}{\pi k_{\alpha}}} e^{\pm i\Theta_{\alpha}(r)} = \frac{\mathcal{F}_{\alpha}(r) \pm i\mathcal{G}_{\alpha}(r)}{2},\tag{19}$$

the scattering states that satisfies incoming boundary conditions, $|\Psi^-_{\alpha,E}\rangle$, with channel radial components $u^-_{\beta,\alpha E}$ specified by Eq. (10), are obtained by the following linear combination of the solutions $|\Psi_{\alpha,E}\rangle$

$$|\Psi_{\alpha,E}^{-}\rangle = \sum_{\beta} |\Psi_{\beta,E}\rangle \left[\frac{1}{\mathbf{B} - i\mathbf{A}}\right]_{\beta,\alpha},\tag{20}$$

where $[\mathbf{A}]_{\beta,\alpha} = [\mathbf{A}(E)]_{\beta,\alpha} = A_{\beta,\alpha E}$ and $[\mathbf{B}]_{\beta,\alpha} = [\mathbf{B}(E)]_{\beta,\alpha} = B_{\beta,\alpha E}$. Indeed, with this choice, the function $\Psi_{\alpha,E}^-$ has only outgoing components in channel α .

$$\Psi_{\alpha,E}^{-} \xrightarrow{r_{N_{e}} \to \infty} \frac{1}{N_{e}} \Upsilon_{\alpha} \sqrt{\frac{2}{\pi k_{\alpha}}} e^{i\Theta_{\alpha}(r_{N_{e}})} + \frac{1}{N_{e}} \sum_{\beta} \sqrt{\frac{2}{\pi k_{\beta}}} e^{-i\Theta_{\beta}(r_{N_{e}})} \left[\frac{\mathbf{B} + i\mathbf{A}}{\mathbf{B} - i\mathbf{A}} \right]_{\beta,\alpha}.$$
(21)

By comparing with Eqs. (9) and (10), the scattering matrix is thus given by

$$S = \frac{B - iA}{B + iA}.$$
 (22)

Notice that, despite the inherent asymmetry between the channel indexes of the matrices A and B (the right index referring to the scattering state as a whole, and the left index referring to a specific channel within that scattering state), the Hermiticity and reality of the Hamiltonian operator requires that the scattering matrix so computed to be unitary. Indeed, the quantity $\operatorname{tr}(|S^{\dagger}S-1|)$ is used as a measure of the numerical accuracy of the whole procedure.

Using this technique, we only need the energies of the box eigenstates, the radial derivative of the box eigenstates (\mathcal{D}_{Φ}) at R_{max} and the Hamiltonian with the last B-Splines. The size of these matrices is substantially small compared to the size of the Hamiltonian matrix. Therefore, the scattering states can be computed immediately after the diagonalization of the box for any system size. Since the scattering states are stored as linked lists, it is possible to select a first coarse energy grid, and refine it on the most relevant regions. This is very useful to resolve any interesting feature without increasing the density of energy points across the whole energy grid.

2.4. Electron angular distributions

Another important addition to the new XCHEM version is the calculation of electron angular distributions. Scattering states representing electron ejection in a particular direction \hat{k} and spin $\sigma,\,|\Psi^-_{\alpha \hat{k} \hat{k} \sigma}\rangle$, can be expressed in terms of the spherical scattering states $|\Psi^-_{\alpha \ell m E}\rangle$, in which the outgoing photoelectron has a well defined orbital angular momentum

$$|\Psi^{-}_{\alpha E \hat{k} \sigma}\rangle = \sum_{\ell m} i^{\ell-1} Y^*_{\ell m}(\hat{k}) e^{-i\sigma_{\ell}(k)} \sum_{S\Sigma} C^{S\Sigma}_{S_{\alpha} \Sigma_{\alpha}, \frac{1}{2} \sigma} |\Psi^{-}_{\alpha \ell m E}\rangle. \tag{23}$$

In a first step, XCHEM provides scattering states in terms of symmetry-adapted spherical harmonics $X_{\ell m}$ instead of the ordinary spherical harmonics $Y_{\ell m}$,

$$X_{\ell 0} = Y_{\ell 0} \tag{24}$$

$$X_{\ell m} = \frac{1}{\sqrt{2}} (Y_{\ell m} + (-1)^m Y_{\ell - m}), \quad m > 0$$
 (25)

$$X_{\ell-m} = \frac{1}{\sqrt{2}i} (Y_{\ell m} - (-1)^m Y_{\ell-m}), \quad m > 0.$$
 (26)

Using the above relations, Eq. (23) can thus be written as

$$|\Psi^{-}_{\alpha E \hat{k} \sigma}\rangle = \sum_{\ell m} i^{\ell-1} Y_{\ell m}^{*}(\hat{k}) e^{-i\sigma_{\ell}(k)} \sum_{S\Sigma} C_{S_{\alpha}\Sigma_{\alpha}, \frac{1}{2}\sigma}^{S\Sigma} \frac{a_{m}}{\sqrt{2}} (|\Psi^{-}_{\alpha X \ell mE}\rangle$$

$$+ib_m|\Psi^-_{\alpha X\ell-mF}\rangle),\tag{27}$$

where $a_m=1$ if m>0, $a_0=\sqrt{2}$, and $a_m=-i(-1)^m$, if m<0, and $b_m=1-\delta_{m0}$. Similarly, XCHEM works with cartesian components of the electronic dipole operator. The corresponding spherical components are obtained by using the standard relations

$$d_1 = -\frac{d_x + id_y}{\sqrt{2}} \tag{28}$$

$$d_0 = d_z \tag{29}$$

$$d_{-1} = \frac{d_x - id_y}{\sqrt{2}}. (30)$$

From equation (27), XCHEM computes molecular frame photoelectron angular distributions (MFPADs) from the expression (see Ref. [60])

$$\frac{dP_{\alpha}}{dEd\hat{k}} = (2S+1)\sum_{j\mu} Y_{j\mu}(\hat{k})B_{j\mu}$$
 (31)

where

$$B_{j\mu} = \sum_{\ell\ell'} \frac{\Pi_{j\ell'}}{\sqrt{4\pi} \Pi_{\ell}} i^{\ell' - \ell} e^{i(\sigma_{\ell} - \sigma_{\ell'})} C_{j0,\ell'0}^{\ell 0}$$
(32)

$$\times \sum_{mm'} C^{\ell~\mu+m'}_{j\,\mu,\ell'm'} \frac{a^*_m a_{m'}}{2} [A_{a\ell\,mE} - i b_m A_{a\ell-mE}] [A^*_{a\ell'm'E} + i b_{m'} A^*_{a\ell'-m'E}],$$

 $\Pi_{ab\cdots}=\sqrt{(2a+1)(2b+1)\cdots}$, and $A_{a\ell^mE}$ is the partial photoionization amplitude, which to first order of perturbation theory is simply given by the dipole transition matrix element connecting the initial bound state and the final continuum state

$$A_{a\ell mE} = \langle \Psi_{a\ell mE}^{-} | \hat{d}_{\mu} | \Psi_{0} \rangle. \tag{33}$$

The new version of the code also provides the asymmetry parameter β through the following equation

$$\beta = -5\sqrt{\frac{2}{5}} \frac{F_2}{F_0},\tag{34}$$

where

$$\begin{split} F_{J} &= \sum_{\ell_{a}, m_{a}, \mu_{a}} \sum_{\ell_{b}, m_{b}, \mu_{b}} \delta_{\mu_{a} + m_{a}, \mu_{b} + m_{b}} (-1)^{J} C_{\ell_{b}0, J0}^{\ell_{a}0} C_{\ell_{a}m_{a}, J}^{\ell_{b}m_{b}} \\ &\times C_{1\mu_{b}, J}^{1\mu_{a}} \sum_{\mu_{a} - \mu_{b}} i^{\ell_{a} - \ell_{b}} e^{i(\sigma_{\ell_{b}} - \sigma_{\ell_{a}})} \langle \Psi_{\alpha \ell_{a} m_{a}E}^{-} | \hat{d}_{\mu_{a}} | \Psi_{0} \rangle^{*} \langle \Psi_{\alpha \ell_{b} m_{b}E}^{-} | \hat{d}_{\mu_{b}} | \Psi_{0} \rangle. \end{split}$$

The β parameter is then used to evaluate the photoelectron angular distribution in the laboratory frame through the equation

$$\frac{d\sigma_{\mu'}}{dEd\Omega} = \frac{\sigma_{\mu'}}{4\pi} [1 + \beta P_2(\cos\theta)],\tag{35}$$

where μ' refers to a photon polarized in the z direction of the laboratory frame, $\sigma_{\mu'}$ is the total cross section, \mathcal{P}_2 is the well known Legendre polynomial and θ is the angle between the laser polarization and the photoelectron.

3. Validation, benchmarking and performance

We have checked the validity of XCHEM-2.0 in different ways. First, by comparing with photoionization cross sections of N_2 [58,57] obtained with the original version of the code. For this, the same basis sets were used. The results are identical to numerical accuracy. The calculated cross sections are also in good agreement with the available experimental ones (see [58,57] and Fig. 2 below). This is specially remarkable in the region of the Hopfield series of N_2 resonances, where, to our knowledge, there is only one more theoretical calculation [40], also in very good agreement with the original XCHEM results. In previous work, we have also compared our calculated cross sections and β parameters for CO [60] and water [61] with those obtained with other

methods and with experiment, finding a reasonable agreement in all cases.

The MFPAD routines have been validated by comparing our calculated MFPADs with previous theoretical ones reported by Lucchese [69] for the CO molecule in a wide range of photoelectron energies (see [60]). The agreement is very good, the differences being much smaller than typical experimental uncertainties. For N_2 , the comparison between our calculated and measured β parameters presented in the following section also shows a good agreement, giving further support to our implementation of these parameters.

In addition to this, we have compared our results for the CO molecule with those obtained with the recently developed ASTRA code [40] by using exactly the same active space and basis sets. For this test we had to use a reduced active space to make it compatible with the one that can be currently employed with the latest version of ASTRA. The results are in perfect agreement.

All the improvements described in the previous section have also led us to significantly reduce storage space by a factor of 10 with respect to the original version, which is one of the key questions to extend XCHEM to larger molecules. In this work we have taken advantage of this fact to study photoionization of pyrazine by including up to l=8, the largest calculation ever performed with XCHEM.

Finally, the new way of obtaining the scattering wave functions described in the previous section allows for a significant reduction in computer time, by a factor of two or three depending on the system and the problem, when one is interested in obtaining a description of these states in a wide range of photoelectron energies or in a dense grid of photoelectron energies without increasing the density of states (i.e., the box size).

At the low photoelectron energies considered in this work, the limitations in molecular size and computational effort are only slightly higher than for excited state calculations performed within the CASSCF and RAS methodologies. This is because the logic of XCHEM 2.0 closely follows that of OpenMOLCAS. The higher price comes from the addition of the monocentric gaussian basis and the computation of integrals involving this basis and the polycentric gaussian basis. The computational cost of integrals involving B-splines is significantly much smaller because they are evaluated analytically.

4. Results and discussion

4.1. Nitrogen molecule

In previous work [57,58], we have reported photoionization cross sections of N_2 in the region of the Hopfield series of resonances, i.e., between the $A^2\Pi_u$ and $B^2\Sigma_u^+$ ionization thresholds. These resonances have been observed in several synchrotron radiation experiments with high energy resolution [70–72] and more recently in attosecond experiments [23]. Here we have evaluated molecular-frame photoelectron angular distributions (MFPADs) and β asymmetry parameters in the same energy region. For this, we have repeated and extended the calculations performed in [57] and [58] by using the new XCHEM-2.0 code.

In these calculations, we have considered photoionization of N₂ leaving the N_2^+ cation in the three lowest electronic states: $X^2\Sigma_g^+$, $A^2\Pi_u$ and $B^2\Sigma_u^+$. The nuclear positions were fixed at the experimental equilibrium geometry (D(N-N) = 1.1 Å). The orbitals used in our calculations have been obtained with MOLPRO [42] by performing a state average Restricted Active Space SCF (SA-RASSCF) that comprises the ground state and the lowest three excited states of the neutral, uses a cc-pVQZ basis set and considers all configurations in which the $1\sigma_g$ and $1\sigma_u$ orbitals are doubly occupied, the $2\sigma_g$, $2\sigma_u$, $3\sigma_g$, $3\sigma_u$, $1\pi_g$ and $1\pi_u$ orbitals can be occupied by an arbitrary number of electrons (complete active space) and the $4\sigma_g$, $4\sigma_u$, $5\sigma_g$, $5\sigma_u$, $6\sigma_g$, $6\sigma_u$, $2\pi_g$, $2\pi_u$, $3\pi_g$, $3\pi_u$, $1\delta_g$ and $1\delta_u$ orbitals can have up to two electrons (restricted active space). These orbitals were then used to describe the $X^2\Sigma^+$, $A^2\Pi$ and $B^2\Sigma^+$ cationic states included in the second term of the close-coupling expansion

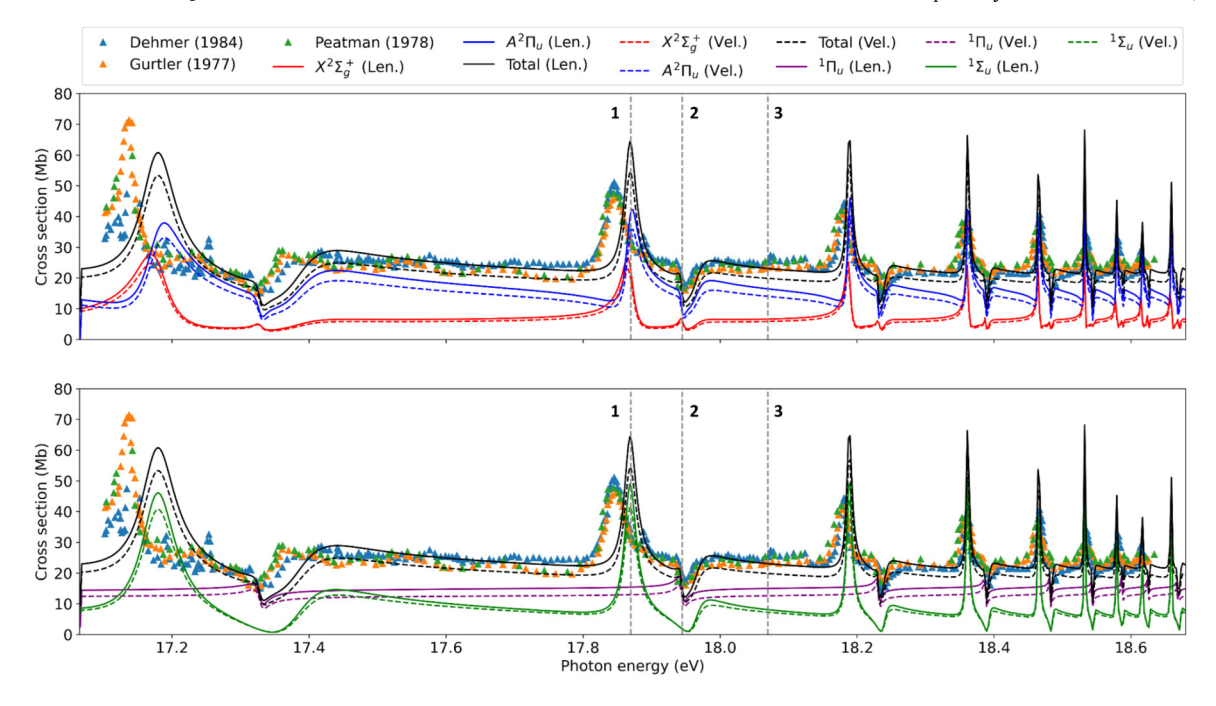


Fig. 1. N_2 Cross section. (a) Partial photoionization cross sections for the $X^2\Sigma_g^+$ (red) and $A^2\Pi_u$ (blue) ionization channels. (b) Partial cross section for the $^1\Sigma_u$ (green) and $^1\Pi_u$ (purple) final symmetries of the system. Total cross section in black. Solid and dashed lines correspond to length and velocity gauges respectively. Triangles are experimental data from Dehmer P. M. et al. (blue), Peatman W. B. et al. (green) and Gürtler P. et al. (orange). The vertical lines labeled as 1, 2 and 3 correspond to 17.87, 17.945 and 18.07 eV photon energies. (For interpretation of the colors in the figure(s), the reader is referred to the web version of this article.)

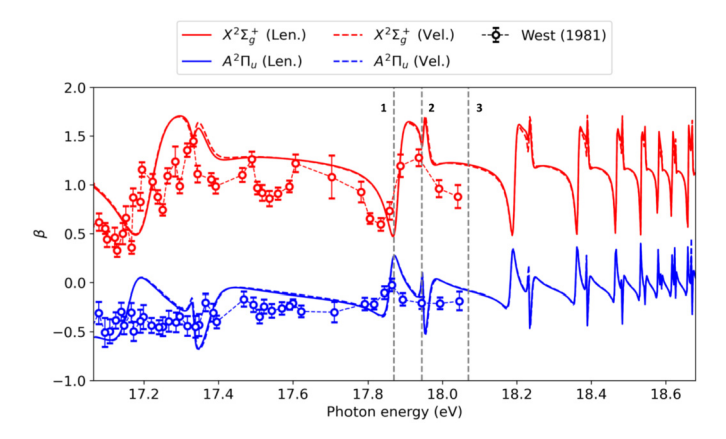


Fig. 2. N_2 **Beta asymmetry parameter.** Beta asymmetry parameter of the $X^2\Sigma_g^+$ (red) and $A^2\Pi_u$ (blue) ionization channels. Circles correspond to experimental data for the first vibrational state obtained by West J. B. et al. [74]. The vertical lines labeled as 1, 2 and 3 correspond to 17.87, 17.945 and 18.07 eV photon energies.

(eq. (1)) by performing the same RASSCF calculation. This approach yields a good description of the considered states as can be checked by comparing the calculated and the experimental ionization energies (experimental values indicated in parentheses), $X^2\Sigma_g^+$: 15.35 eV (15.58 eV), $A^2\Pi_u$: 16.84 eV (17 eV) and $B^2\Sigma_u^+$: 18.52 eV (18.8 eV). To account for the small difference between the theoretical and experimental ionization potentials, the theoretical data were shifted +0.23 eV. The set of monocentric GABS used to describe the photoelectron is placed at the center of mass of the molecule. It consists of a set of 390 B-splines of order 7 defined in a linear grid between $R_0=7$ a.u. and $R_{max}=200$ a.u. with $I\leq 3$, and a set of 22 even-tempered Gaussian functions $\mathcal{G}_i^M(r)\propto r^{2k+l}e^{-\alpha_i r^2}$, where $\alpha_i=\alpha_0\beta^i$ ($\alpha_0=0.01,\beta=1.46,i=0,1,...,21$), $I\leq 3$ and I_0 and I_0 are the ground state and the lowest three excited states of the neutral molecule.

The calculated total cross sections, shown in Fig. 1, are nearly indistinguishable from those of Ref. [57]. For completeness, Fig. 1 also shows the cross sections obtained from synchrotron radiation experiments [70,71,73], as well as the calculated partial cross sections for both $X^2\Sigma_g^+$ and $A^2\Pi_u$ channels (panel a) and the contribution from continuum states of $^1\Sigma_u$ and $^1\Pi_u$ symmetries (the only accessible ones within the dipole approximation). Apart from the lowest Feshbach resonance, which is a bit shifted, probably due to the neglect of nuclear motion in the present calculations, the agreement with the experimental data is reasonably good. The difference between results obtained in the length and velocity gauges is very small, thus indicating that our description of the electronic wave function in such a highly correlated region is very good. For more details about the meaning of the different structures observed in the calculated spectra, we refer the reader to Refs. [57,58].

Fig. 2 shows the calculated β asymmetry parameter and the corresponding experimental values obtained by West et al. [74] for the lowest vibrational state. The agreement is quite remarkable irrespective of the chosen gauges. The values of β clearly indicate that the preferred direction of photoelectron ejection with respect to the light polarization axis is very different in the $X^2\Sigma_g^+$ or $A^2\Pi_u$ channels. When the N_2^+ cation is left in the $X^2\Sigma_a^+$ state, the electron is preferentially ejected along the polarization direction, while the opposite is observed when the cation is left in the $A^2\Pi_{ij}$ state. The degree of anisotropy in the electron ejection (i.e., how much β departs from zero) changes abruptly in the vicinity of the Feshbach resonances. These abrupt variations are very well represented by the calculations, which is remarkable in view of the high sensitivity of the β parameters to electron correlation effects. Similar abrupt variations of the β asymmetry parameter close to Feshbach resonances have also been reported for the CO [60] and water [75] molecules.

Fig. 3 shows normalized MFPADs in length gauge (those in velocity gauge are indistinguishable) for the different final cationic states and polarization directions at the photon energies represented with vertical lines in Fig. 1 and 2. When the cation is left in the $X^2\Sigma_g^+$ state, the preferred electron ejection direction roughly follows the polarization

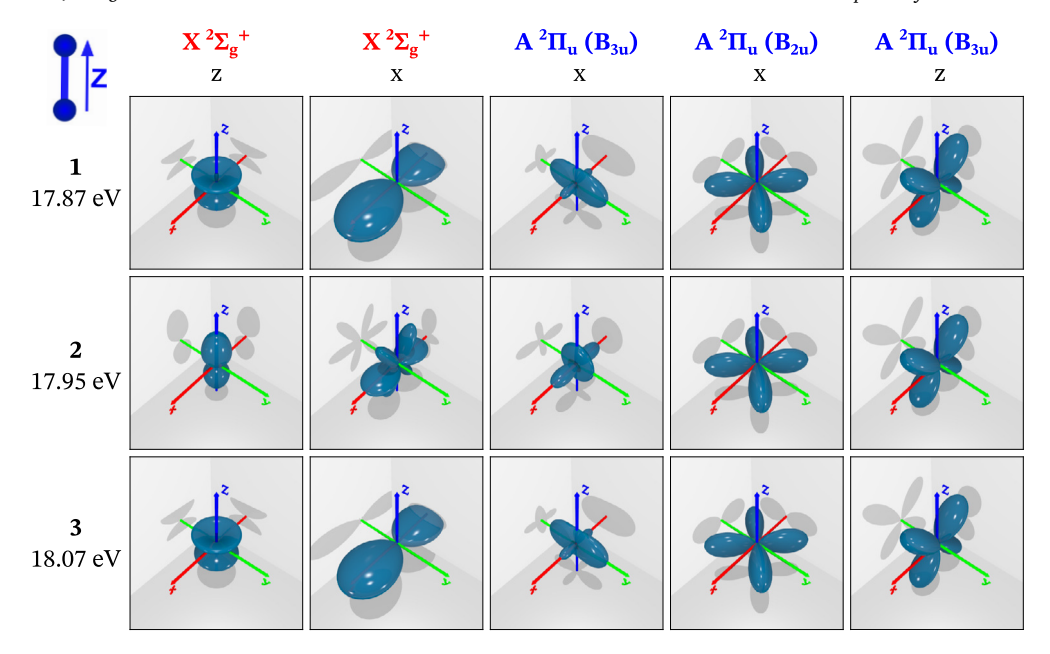


Fig. 3. N_2 MFPAD Normalized MFPAD for the $X^2\Sigma_g^+$ and $A^2\Pi_u$ ionization channels and x ($^1\Pi_u$) and z ($^1\Sigma_u$) polarization directions at 17.87, 17.945 and 18.07 eV of photon energies.

direction irrespective of the chosen energy, with a noticeable exception: the MFPAD for x polarization (i.e., polarization perpendicular to the molecular axis) at 17.95 eV (vertical line 2 in Fig. 1). This is due to differences in electron correlation between the resonance populated at this energy and that populated at 17.87 eV (vertical line 1), and between the former and the non resonant continuum at 18.07 eV (vertical line 3). This change in electron correlation is also at the origin of the abrupt change of the β parameter in the same energy region. When the cation is left in $A^2\Pi_{\mu}$ state, electron emission follows neither the polarization direction nor the internuclear axis, except for the $\Pi_{\mu x}$ component ($B_{3u,x}$ in D_{2h} symmetry) at 17.95 eV (vertical line 2) for xpolarization (i.e., perpendicular to the molecular axis). In this case, one observes the largest variations of the MFPADs when moving from region 1 to 2 and then to 3, again as a consequence of the different role played by electron correlation in the corresponding final states. However, similar abrupt changes in the MFPADs with energy are observed neither for the other Π component with x polarization nor for z polarization (i.e., parallel to the molecular axis). These results show that, in the vicinity of Feshbach resonances, it is almost impossible to guess the preferred electron emission directions without explicitly performing fully correlated calculations.

4.2. Pyrazine molecule

As a first attempt to describe photoionization in the vicinity of Feshbach resonances in significantly larger molecules, we have considered pyrazine. Pyrazine is an aromatic heterocycle, isomer of pyrimidine, a constituent of the nucleo-bases cytosine, thymine and uracil. Even though it is not itself a nucleobasis, it has been used as a model for pyrimidinic nucleobases thanks to its high D_{2h} symmetry [76,77]. We have focused on the energy region delimited by the first and third ionization thresholds, where we expect to encounter a large number of these resonances. Therefore, this is the first step towards investigating their potential role in the photoionization of biologically relevant molecules. Rydberg states of pyrazine lying below the first ionization threshold have been investigated in previous works [78,79], but, to our knowledge, never above the ionization threshold. Asymmetry parameters have been measured experimentally [80] for photon energies higher than 13 eV, and theoretically [81] in the range 0-30 eV of photoelectron kinetic energy, but without the energy resolution required to perform a detailed analysis of the Feshbach resonances.

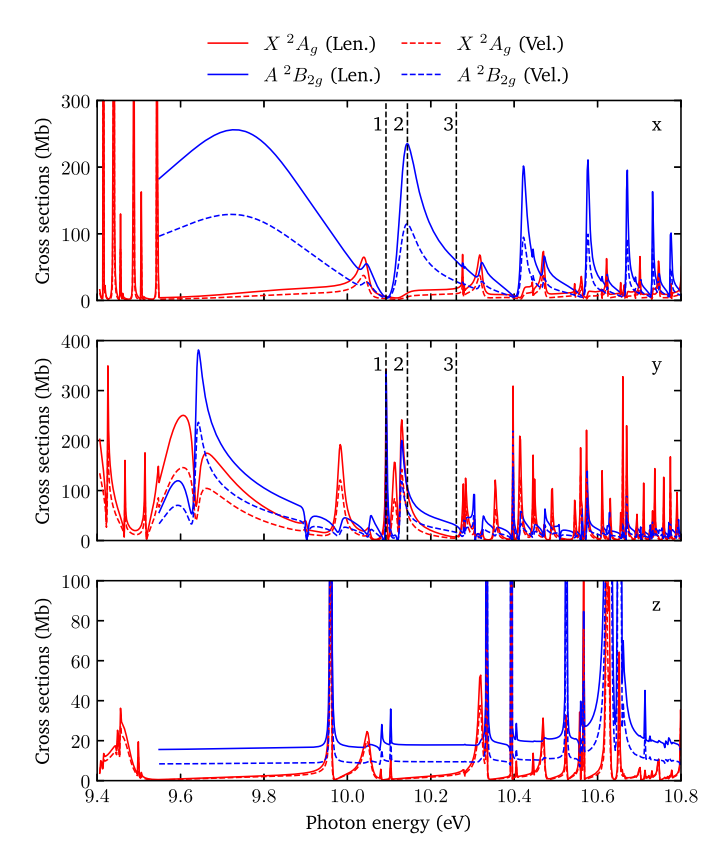


Fig. 4. Partial cross sections for the single-photon ionization of pyrazine for the two lowest ionization channels \tilde{X}^2A_g (red) and \tilde{A}^2B_{2g} (blue) between the first and third ionization thresholds. Top, middle and bottom panels: partial cross sections for polarization along x, y and z directions, respectively. We compare the length (solid line) and velocity (dashed line) gauges. The photon energy was shifted by 0.92 eV to match the experimental ionization energy.

We have performed an MP2 geometry optimization of pyrazine and then considered that the molecule remains fixed at the equilibrium geometry. We have considered photon energies for which the pyrazine cation can only be left in the lowest electronic states (parent ions),

namely, \tilde{X}^2A_g , \tilde{A}^2B_{2g} , \tilde{B}^2B_{2u} , \tilde{C}^2B_{3g} and \tilde{D}^2B_{1u} . These are also the target states included in the second term of the close coupling expansion given (eq. (1)). We have used polycentric orbitals and parent ion states resulting from a state-averaged SA-CASSCF(9,8) calculation using the cc-pVTZ basis set, including all the above-mentioned cationic states. The active space includes the occupied orbitals $1b_{3u}(\pi)$, $1b_{2g}(\pi)$, $5b_{1u}(n)$, $1b_{1g}(\pi)$ and $6a_g(n)$; and the virtual orbitals $2b_{3u}(\pi^*)$, $1a_u(\pi^*)$ and $2b_{2a}(\pi^*)$, i.e., we have included all the n, π and π^* orbitals. The ground state of neutral pyrazine has been calculated by using the same set of polycentric orbitals resulting from the above-mentioned SA-CASSCF calculation. It has also been included in the first term of the close-coupling expansion (eq. (1)). The calculated ionization energies are 8.49, 8.63, 9.90, 10.02 and 12.26 eV, to be compared with the experimental values 9.4 (8.7-10.0), 10.2 (10.0-10.8), 11.3 (10.8-11.4), 11.8 (11.4-12.8) and 13.4 (12.8-13.8) eV from Holland et al. [82], where the numbers within parenthesis indicate the lower and upper binding energies of the observed bands. We have used a GABS basis consisting of 380 B-splines of 7th order defined in a linear grid between $R_0 = 8.0$ a.u. and $R_{\text{max}} = 200$ a.u. with $l \le 8$, and a set of even-tempered Gaussian functions $G_i(r) \propto r^{l+2k} e^{-\alpha_i r^2}$ with $\alpha_i = \alpha_0 \beta^i$ $(\alpha_0 = 0.01, \beta = 1.46, \text{ for } i = 0, 1, \dots, 21) \text{ for each pair of } l \le 8 \text{ and } k \le 0.$

We have computed single photoionization cross sections and asymmetry parameters for the \tilde{X}^2A_g and \tilde{A}^2B_{2g} ionization channels for photon energies from 9.4 to 10.8 eV. In the following, we will consider that the molecule lies in the xy plane with the nitrogen atoms located along the y axis. Fig. 4 shows the partial photoionization cross sections for the \tilde{X}^2A_g and \tilde{A}^2B_{2g} channels for the three polarization directions of the electric field (x, y and z). Although the differences between the results obtained in length and velocity gauges are more pronounced than for N_2 , suggesting that more ionization channels should have probably been included, the corresponding curves exhibit the same features and basically differ by a global scaling factor. Therefore, one can trust that, apart from the absolute value, all the observed features are correctly reproduced.

First of all, as can be seen, the cross sections are roughly an order of magnitude larger than for N_2 , except for the z polarization case (i.e., perpendicular to the molecular plane), which is expected due to the larger size of pyrazine. The cross sections for z polarization are roughly an order of magnitude smaller due to the fact that the electron density is delocalized all over the molecule and is mainly localized in the vicinity of the molecular plane, which leads to much larger dipole transition amplitudes for polarization directions parallel to this plane. As can be seen, the investigated energy region is crowded with Feshbach resonances, some of them broader than 0.1 eV, e.g., the resonances at around 10.1 eV photon energy for x polarization and at around 9.7 eV for y polarization. Therefore, despite the expected vibrational spreading, one may expect these resonances to be observed experimentally. We will first focus our attention on the x polarization. In the $\tilde{A}^2 B_{2\sigma}$ channel, we can clearly distinguish two series of Feshbach resonances. Elements of this two series appear as pairs, with the wider resonances always appearing first. We see that as we approach the third ionization threshold, the resonances become narrower and closer to each other, suggesting that they come from the autoionization of Rydberg states. In contrast, the \tilde{X}^2A_g partial cross section exhibits a single series of resonances, whose positions approximately coincide with those of the narrow series observed in the \tilde{A}^2B_{2g} channel. For y polarization, for which the absolute value of the cross section is comparable to the x polarization case, other resonances show up, leading to different asymmetric peaks. The same occurs for z polarization, although in this case the contribution of the resonances to the total cross section would be barely visible due to the much smaller value of the cross section.

Fig. 5 shows the calculated asymmetry parameters for the \tilde{X}^2A_g and \tilde{A}^2B_{2g} ionization channels. Length and velocity gauges are almost superimposed to each other. As in N₂, one can see that the β parameter, and consequently the preferred electron emission direction, depends very much on the state in which the remaining molecular cation is

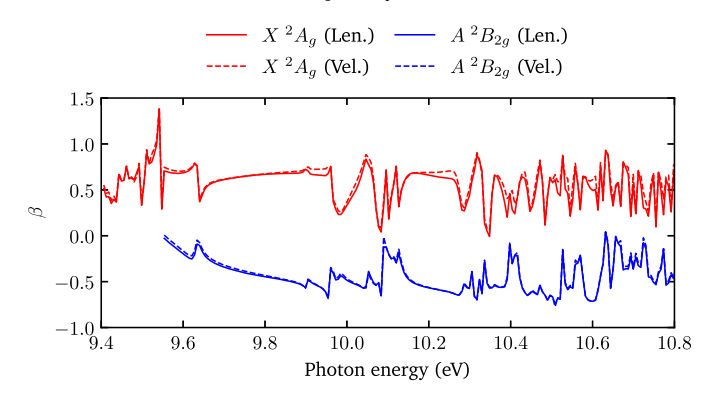


Fig. 5. Asymmetry parameter for the pyrazine molecule between the first and third ionization thresholds for the two lowest ionizations channels \tilde{X}^2A_g (red) and \tilde{A}^2B_{2g} (blue). Length gauge appears as solid lines, while velocity gauge as dashed lines. The photon energy was shifted by 0.92 eV to match the experimental ionization energy.

left. Also, the presence of Feshbach resonances causes the β parameter, hence the degree of anisotropy in electron emission, to change abruptly.

Finally, Fig. 6 shows the calculated MFPADs for the \tilde{X}^2A_g and $\tilde{A}^2 B_{2\sigma}$ ionization channels for x and y polarization directions, which are associated to the largest ionization cross sections. We have only plotted the results obtained at the three photon energies indicated by vertical lines 1, 2 and 3 in Fig. 4 (10.09 eV, 10.14 eV and 10.26 eV, respectively). In general, for either polarization, the MFPADs depend very much on the final state of the cation and the preferred electron emission direction does not coincide with the polarization direction. Interestingly, in most cases, the preferred electron emission directions do not lie in the molecular plane, despite that the polarization directions do. Furthermore, the MFPADs exhibit a multilobe pattern that changes abruptly when one crosses a particular resonance, e.g., when moving from 10.09 eV (vertical line 1 in Fig. 4) to 10.26 eV (vertical line 3 in Fig. 4). Interestingly, in the case of the \tilde{X}^2A_g channel for x polarization, we observe a change in the directions of emission from the xzplane (perpendicular to the pyrazine ring) to the xy plane (the pyrazine ring). In the case of the \tilde{A}^2B_{2g} ionization channel and x polarization, we can see the shrinking and enlargement of lobes as we move from below the resonance to above it. The latter two changes are not observed for y polarization.

5. Conclusion

The XCHEM code was originally designed to represent the electronic continuum of molecules in those regions of the spectrum where electron correlation plays a major role, as in the vicinity of the ionization threshold and Feshbach resonances. The success of this implementation for small molecules has led us to improve its performance in several aspects, which now allows for the description of resonant molecular photoionization in larger systems. The main improvements concern (i) the augmentation procedures used to build N_{ρ} -electron configurations from $(N_{\rho}-1)$ ones, (ii) the way data are stored, (iii) a more efficient removal of linear dependencies and (iv) a more efficient solution of the scattering equations. All of which has led us to significantly reduce computer time, and storage space by a factor of 10, with respect to the original version. In addition, (v) we have included the possibility to evaluate photoelectron angular distributions in both the laboratory and molecular frames. The performance of the new version of the code, XCHEM-2.0, has been demonstrated in the N_2 and pyrazine molecules, for which we have provided photoionization cross sections and photoelectron angular distributions in the region of Feshbach resonances. We hope that the new code will allow for systematic investigations of resonant photoionization of molecules containing up to around 10 atoms by including electron correlation effects at a level similar to that provided by state-of-the-art quantum chemistry packages for bound states.

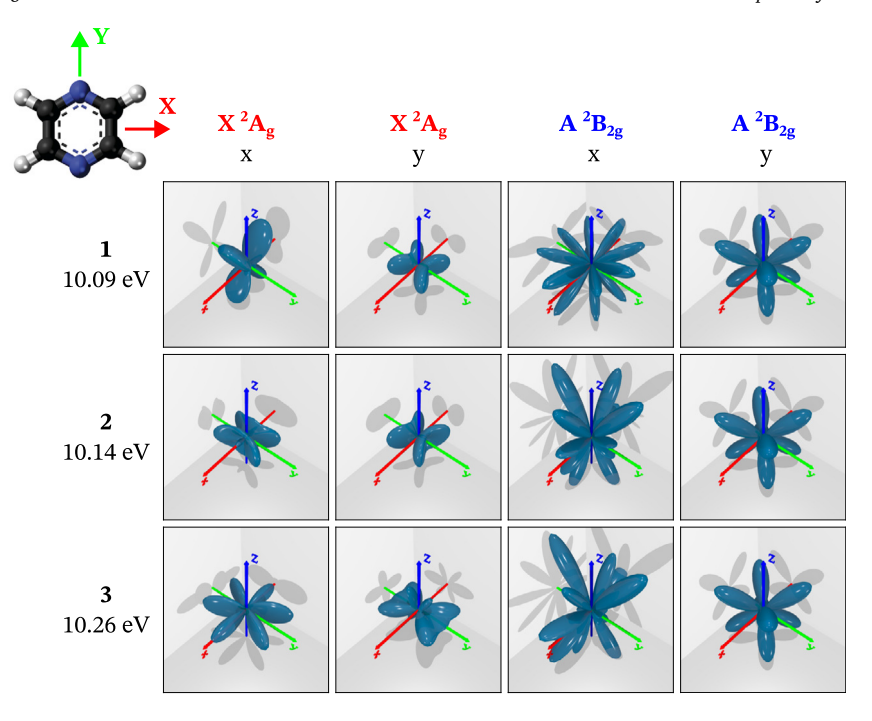


Fig. 6. XCHEM computed MFPADs for the \tilde{X}^2A_g and \tilde{A}^2B_{2g} ionization channels of the pyrazine molecule for x and y polarizations at 10.09, 10.14 and 10.26 eV photon energy. The photon energy was shifted by 0.92 eV to match the experimental ionization energy.

Declaration of competing interest

The authors declare that they have no known competing financial interests or personal relationships that could have appeared to influence the work reported in this paper.

Data availability

We have provided a gitlab link with the code.

Acknowledgements

This publication is based upon work from COST Action AttoChem, CA18222 supported by COST (European Cooperation in Science and Technology). All calculations were performed at the Mare Nostrum Supercomputer of the Red Española de Supercomputación (BSC-RES) and the Centro de Computación Científica de la Universidad Autónoma de Madrid (CCC-UAM). Work supported by the Synergy Grant of the European Research Council TOMATTO (ref. 951224), the projects PDC2021-121073-I00, PID2019-105458RB-I00 and PID2019-106732GB-I00 funded by MCIN/AEI/10.13039/501100011033 and by the European Union "NextGenerationEU"/PRTRMICINN programs, the "Severo Ochoa" Programme for Centres of Excellence in R&D (CEX2020-001039-S), and the "María de Maeztu" Programme for Units of Excellence in R&D (CEX2018-000805-M). L.A. acknowledges the DOE CAREER grant No. DE-SC0020311V and the NSF grant PHY-1912507. J.B. thanks the MICINN for the FPI grant (BES-2017-081521) related to the project FIS2016-77889-R and P.F-M the MICINN for the FPU grant (FPU-2016-05453) related to the project FIS2016-77889-R.

References

- C. Marante, M. Klinker, I. Corral, J. González-Vázquez, L. Argenti, F. Martín, Hybrid-basis close-coupling interface to quantum chemistry packages for the treatment of ionization problems, J. Chem. Theory Comput. 13 (2) (2017) 499–514, https://doi.org/10.1021/acs.jctc.6b00907.
- [2] J. Li, J. Lu, A. Chew, S. Han, J. Li, Y. Wu, H. Wang, S. Ghimire, Z. Chang, Attosecond science based on high harmonic generation from gases and solids, Nat. Commun. 11 (1) (2020) 2748, https://doi.org/10.1038/s41467-020-16480-6.

- [3] M. Nisoli, P. Decleva, F. Calegari, A. Palacios, F. Martín, Attosecond electron dynamics in molecules, Chem. Rev. 117 (16) (2017) 10760–10825, https://doi.org/10.1021/acs.chemrev.6b00453.
- [4] F. Calegari, G. Sansone, S. Stagira, C. Vozzi, M. Nisoli, Advances in attosecond science, J. Phys. B, At. Mol. Opt. Phys. 49 (6) (2016) 062001, https://doi.org/10.1088/0953-4075/49/6/062001.
- [5] F. Frank, C. Arrell, T. Witting, W.A. Okell, J. McKenna, J.S. Robinson, C.A. Haworth, D. Austin, H. Teng, I.A. Walmsley, J.P. Marangos, J.W.G. Tisch, Invited review article: technology for attosecond science, review of scientific instruments 83 (7) (2012) 071101, https://doi.org/10.1063/1.4731658.
- [6] F. Krausz, M. Ivanov, Attosecond physics, Rev. Mod. Phys. 81 (1) (2009) 163–234, https://doi.org/10.1103/RevModPhys.81.163.
- [7] M.F. Kling, M.J. Vrakking, Attosecond electron dynamics, Annu. Rev. Phys. Chem. 59 (1) (2008) 463–492, https://doi.org/10.1146/annurev.physchem.59.032607. 093532.
- [8] P.M. Paul, E.S. Toma, P. Breger, G. Mullot, F. Augé, Ph. Balcou, H.G. Muller, P. Agostini, Observation of a train of attosecond pulses from high harmonic generation, Science 292 (5522) (2001) 1689–1692, https://doi.org/10.1126/science.1059413.
- [9] M. Hentschel, R. Kienberger, C. Spielmann, G.A. Reider, N. Milosevic, T. Brabec, P. Corkum, U. Heinzmann, M. Drescher, F. Krausz, Attosecond metrology, Nature 414 (6863) (2001) 509–513, https://doi.org/10.1038/35107000.
- [10] T. Barillot, O. Alexander, B. Cooper, T. Driver, D. Garratt, S. Li, A. Al Haddad, A. Sanchez-Gonzalez, M. Agåker, C. Arrell, M.J. Bearpark, N. Berrah, C. Bostedt, J. Bozek, C. Brahms, P.H. Bucksbaum, A. Clark, G. Doumy, R. Feifel, L.J. Frasinski, S. Jarosch, A.S. Johnson, L. Kjellsson, P. Kolorenč, Y. Kumagai, E.W. Larsen, P. Matia-Hernando, M. Robb, J.-E. Rubensson, M. Ruberti, C. Sathe, R.J. Squibb, A. Tan, J.W.G. Tisch, M. Vacher, D.J. Walke, T.J.A. Wolf, D. Wood, V. Zhaunerchyk, P. Walter, T. Osipov, A. Marinelli, T.J. Maxwell, R. Coffee, A.A. Lutman, V. Averbukh, K. Ueda, J.P. Cryan, J.P. Marangos, Correlation-driven transient hole dynamics resolved in space and time in the isopropanol molecule, Phys. Rev. X 11 (3) (2021) 031048, https://doi.org/10.1103/PhysRevX.11.031048.
- [11] J. Duris, S. Li, T. Driver, E.G. Champenois, J.P. MacArthur, A.A. Lutman, Z. Zhang, P. Rosenberger, J.W. Aldrich, R. Coffee, G. Coslovich, F.-J. Decker, J.M. Glownia, G. Hartmann, W. Helml, A. Kamalov, J. Knurr, J. Krzywinski, M.-F. Lin, J.P. Marangos, M. Nantel, A. Natan, J.T. O'Neal, N. Shivaram, P. Walter, A.L. Wang, J.J. Welch, T.J.A. Wolf, J.Z. Xu, M.F. Kling, P.H. Bucksbaum, A. Zholents, Z. Huang, J.P. Cryan, A. Marinelli, Tunable isolated attosecond X-ray pulses with gigawatt peak power from a free-electron laser, Nat. Photonics 14 (1) (2020) 30–36, https://doi.org/10.1038/s41566-019-0549-5.
- [12] H.-S. Kang, C.-K. Min, H. Heo, C. Kim, H. Yang, G. Kim, I. Nam, S.Y. Baek, H.-J. Choi, G. Mun, B.R. Park, Y.J. Suh, D.C. Shin, J. Hu, J. Hong, S. Jung, S.-H. Kim, K. Kim, D. Na, S.S. Park, Y.J. Park, J.-H. Han, Y.G. Jung, S.H. Jeong, H.G. Lee, S. Lee, W.-W. Lee, B. Oh, H.S. Suh, Y.W. Parc, S.-J. Park, M.H. Kim, N.-S. Jung, Y.-C. Kim, M.-S. Lee, B.-H. Lee, C.-W. Sung, I.-S. Mok, J.-M. Yang, C.-S. Lee, H. Shin, J.H. Kim, Y. Kim, J.H. Lee, S.-Y. Park, J. Kim, J. Park, I. Eom, S. Rah, S. Kim, K.H. Nam, J. Park, J. Park, S. Kim, S. Kwon, S.H. Park, K.S. Kim, H. Hyun, S.N. Kim, S. Kim

- S.-m. Hwang, M.J. Kim, C.-y. Lim, C.-J. Yu, B.-S. Kim, T.-H. Kang, K.-W. Kim, S.-H. Kim, H.-S. Lee, H.-S. Lee, K.-H. Park, T.-Y. Koo, D.-E. Kim, I.S. Ko, Hard X-ray free-electron laser with femtosecond-scale timing jitter, Nat. Photonics 11 (11) (2017) 708–713, https://doi.org/10.1038/s41566-017-0029-8.
- [13] A.A. Lutman, R. Coffee, Y. Ding, Z. Huang, J. Krzywinski, T. Maxwell, M. Messer-schmidt, H.-D. Nuhn, Experimental demonstration of femtosecond two-color X-ray free-electron lasers, Phys. Rev. Lett. 110 (13) (2013) 134801, https://doi.org/10.1103/PhysRevLett.110.134801.
- [14] O. Zatsarinny, K. Bartschat, The B-spline R-matrix method for atomic processes: application to atomic structure, electron collisions and photoionization, J. Phys. B, At. Mol. Opt. Phys. 46 (11) (2013) 112001, https://doi.org/10.1088/0953-4075/ 46/11/112001.
- [15] T. Carette, J.M. Dahlström, L. Argenti, E. Lindroth, Multiconfigurational Hartree-Fock close-coupling ansatz: application to the argon photoionization cross section and delays, Phys. Rev. A 87 (2) (2013) 023420, https://doi.org/10.1103/PhysRevA. 87 023420
- [16] L. Argenti, R. Pazourek, J. Feist, S. Nagele, M. Liertzer, E. Persson, J. Burgdörfer, E. Lindroth, Photoionization of helium by attosecond pulses: extraction of spectra from correlated wave functions, Phys. Rev. A 87 (5) (2013) 053405, https://doi.org/10.1103/PhysRevA.87.053405.
- [17] P.G. Burke, R-Matrix Theory of Atomic Collisions: Application to Atomic, Molecular and Optical Processes, Springer Series on Atomic, Optical, and Plasma Physics, vol. 61, Springer, Berlin, Heidelberg, 2011.
- [18] J. Tennyson, Electron-molecule collision calculations using the R-matrix method, Phys. Rep. 491 (2) (2010) 29–76, https://doi.org/10.1016/j.physrep.2010.02.001.
- [19] M. Stener, P. Decleva, Photoionization of first and second row hydrides by the B-spline one-centre expansion density functional method, J. Electron Spectrosc. Relat. Phenom. 94 (1) (1998) 195–209, https://doi.org/10.1016/S0368-2048(98)00186-0
- [20] D. Toffoli, P. Decleva, Multiphoton core ionization dynamics of polyatomic molecules, J. Phys. B, At. Mol. Opt. Phys. 46 (14) (2013) 145101, https://doi.org/ 10.1088/0953-4075/46/14/145101.
- [21] G. Grell, O. Kühn, S.I. Bokarev, Multireference quantum chemistry protocol for simulating autoionization spectra: test of ionization continuum models for the neon atom, Phys. Rev. A 100 (4) (2019) 042512, https://doi.org/10.1103/PhysRevA.100. 042512
- [22] G. Grell, S.I. Bokarev, Multi-reference protocol for (auto)ionization spectra: application to molecules, J. Chem. Phys. 152 (7) (2020) 074108, https://doi.org/10.1063/ 1.5142251
- [23] M. Reduzzi, W.-C. Chu, C. Feng, A. Dubrouil, J. Hummert, F. Calegari, F. Frassetto, L. Poletto, O. Kornilov, M. Nisoli, C.-D. Lin, G. Sansone, Observation of autoionization dynamics and sub-cycle quantum beating in electronic molecular wave packets, J. Phys. B, At. Mol. Opt. Phys. 49 (6) (2016) 065102, https://doi.org/10.1088/0953-4075/49/6/065102
- [24] X. Gong, S. Heck, D. Jelovina, C. Perry, K. Zinchenko, R. Lucchese, H.J. Wörner, Attosecond spectroscopy of size-resolved water clusters, Nature 609 (7927) (2022) 507–511, https://doi.org/10.1038/s41586-022-05039-8.
- [25] H. Ahmadi, E. Plésiat, M. Moioli, F. Frassetto, L. Poletto, P. Decleva, C.D. Schröter, T. Pfeifer, R. Moshammer, A. Palacios, F. Martin, G. Sansone, Attosecond photoionisation time delays reveal the anisotropy of the molecular potential in the recoil frame, Nat. Commun. 13 (1) (2022) 1242, https://doi.org/10.1038/s41467-022-28783-x.
- [26] E. Plésiat, M. Lara-Astiaso, P. Decleva, A. Palacios, F. Martín, Real-time imaging of ultrafast charge dynamics in tetrafluoromethane from attosecond pump-probe photoelectron spectroscopy, Chem. Eur. J. 24 (46) (2018) 12061–12070, https:// doi.org/10.1002/chem.201802788.
- [27] F. Calegari, D. Ayuso, A. Trabattoni, L. Belshaw, S.D. Camillis, S. Anumula, F. Frassetto, L. Poletto, A. Palacios, P. Decleva, J.B. Greenwood, F. Martín, M. Nisoli, Ultrafast electron dynamics in phenylalanine initiated by attosecond pulses, Science 346 (6207) (2014) 336–339, https://doi.org/10.1126/science.1254061.
- [28] S. Haessler, B. Fabre, J. Higuet, J. Caillat, T. Ruchon, P. Breger, B. Carré, E. Constant, A. Maquet, E. Mével, P. Salières, R. Taïeb, Y. Mairesse, Phase-resolved attosecond near-threshold photoionization of molecular nitrogen, Phys. Rev. A 80 (1) (2009) 011404, https://doi.org/10.1103/PhysRevA.80.011404.
- [29] N. Douguet, B.I. Schneider, L. Argenti, Application of the complex Kohn variational method to attosecond spectroscopy, Phys. Rev. A 98 (2) (2018) 023403, https://doi.org/10.1103/PhysRevA.98.023403.
- [30] J. Jose, R.R. Lucchese, T.N. Rescigno, Interchannel coupling effects in the valence photoionization of SF6, J. Chem. Phys. 140 (20) (2014) 204305, https://doi.org/10. 1063/1.4876576.
- [31] T.N. Rescigno, W.A. Isaacs, A.E. Orel, H.-D. Meyer, C.W. McCurdy, Theoretical study of resonant vibrational excitation of CO₂ by electron impact, Phys. Rev. A 65 (3) (2002) 032716, https://doi.org/10.1103/PhysRevA.65.032716.
- [32] B.I. Schneider, T.N. Rescigno, C.W. McCurdy, Resonant vibrational excitation of H₂CO by low-energy electron impact, Phys. Rev. A 42 (1990) 3132–3134, https://doi.org/10.1103/PhysRevA.42.3132, https://link.aps.org/doi/10.1103/PhysRevA.42.3132
- [33] C.W. McCurdy, T.N. Rescigno, Collisions of electrons with polyatomic molecules: electron-methane scattering by the complex Kohn variational method, Phys. Rev. A 39 (9) (1989) 4487–4493, https://doi.org/10.1103/PhysRevA.39.4487.

- [34] R.R. Lucchese, A. Lafosse, J.C. Brenot, P.M. Guyon, J.C. Houver, M. Lebech, G. Raseev, D. Dowek, Polar and azimuthal dependence of the molecular frame photoelectron angular distributions of spatially oriented linear molecules, Phys. Rev. A 65 (2) (2002) 020702, https://doi.org/10.1103/PhysRevA.65.020702.
- [35] R.R. Lucchese, K. Takatsuka, V. McKoy, Applications of the Schwinger variational principle to electron-molecule collisions and molecular photoionization, Phys. Rep. 131 (3) (1986) 147–221, https://doi.org/10.1016/0370-1573(86)90147-X.
- [36] R.E. Stratmann, R.R. Lucchese, A graphical unitary group approach to study multiplet specific multichannel electron correlation effects in the photoionization of O2, J. Chem. Phys. 102 (21) (1995) 8493–8505, https://doi.org/10.1063/1.468841.
- [37] R.E. Stratmann, R.W. Zurales, R.R. Lucchese, Multiplet-specific multichannel electron-correlation effects in the photoionization of NO, J. Chem. Phys. 104 (22) (1996) 8989–9000, https://doi.org/10.1063/1.471632.
- [38] Z. Mašín, J. Benda, J.D. Gorfinkiel, A.G. Harvey, J. Tennyson, UKRmol+: a suite for modelling electronic processes in molecules interacting with electrons, positrons and photons using the R-matrix method, Comput. Phys. Commun. 249 (2020) 107092, https://doi.org/10.1016/j.cpc.2019.107092.
- [39] A. Scrinzi, tRecX an environment for solving time-dependent Schrödinger-like aproblems, Comput. Phys. Commun. 270 (2022) 108146, https://doi.org/10.1016/ j.cpc.2021.108146, arXiv:2101.08171.
- [40] J.M. Randazzo, C. Marante, S. Chattopadhyay, B.I. Schneider, J. Olsen, L. Argenti Astra, Transition-density-matrix approach to molecular ionization, Phys. Rev. Res. 5 (2023) 043115, https://doi.org/10.1103/PhysRevResearch.5.043115, https://link.aps.org/doi/10.1103/PhysRevResearch.5.043115.
- [41] F. Aquilante, J. Autschbach, A. Baiardi, S. Battaglia, V.A. Borin, L.F. Chibotaru, I. Conti, L. De Vico, M. Delcey, I. Fdez Galván, N. Ferré, L. Freitag, M. Garavelli, X. Gong, S. Knecht, E.D. Larsson, R. Lindh, M. Lundberg, P.Å. Malmqvist, A. Nenov, J. Norell, M. Odelius, M. Olivucci, T.B. Pedersen, L. Pedraza-González, Q.M. Phung, K. Pierloot, M. Reiher, I. Schapiro, J. Segarra-Martí, F. Segatta, L. Seijo, S. Sen, D.-C. Sergentu, C.J. Stein, L. Ungur, M. Vacher, A. Valentini, V. Veryazov, Modern quantum chemistry with [Open]Molcas, J. Chem. Phys. 152 (21) (2020) 214117, https://doi.org/10.1063/5.0004835.
- [42] H.-J. Werner, P.J. Knowles, G. Knizia, F.R. Manby, M. Schütz, Molpro: a general-purpose quantum chemistry program package, WIREs Comput. Mol. Sci. 2 (2) (2012) 242–253, https://doi.org/10.1002/wcms.82, https://onlinelibrary.wiley.com/doi/abs/10.1002/wcms.82.
- [43] G.M.J. Barca, C. Bertoni, L. Carrington, D. Datta, N. De Silva, J.E. Deustua, D.G. Fedorov, J.R. Gour, A.O. Gunina, E. Guidez, T. Harville, S. Irle, J. Ivanic, K. Kowalski, S.S. Leang, H. Li, W. Li, J.J. Lutz, I. Magoulas, J. Mato, V. Mironov, H. Nakata, B.Q. Pham, P. Piecuch, D. Poole, S.R. Pruitt, A.P. Rendell, L.B. Roskop, K. Ruedenberg, T. Sattasathuchana, M.W. Schmidt, J. Shen, L. Slipchenko, M. Sosonkina, V. Sundriyal, A. Tiwari, J.L. Galvez Vallejo, B. Westheimer, M. Wloch, P. Xu, F. Zahariev, M.S. Gordon, Recent developments in the general atomic and molecular electronic structure system, J. Chem. Phys. 152 (15) (2020) 154102, https://doi.org/10.1063/5.0005188, http://aip.scitation.org/doi/10.1063/5.0005188.
- [44] K. Aidas, C. Angeli, K.L. Bak, V. Bakken, R. Bast, L. Boman, O. Christiansen, R. Cimiraglia, S. Coriani, P. Dahle, E.K. Dalskov, U. Ekström, T. Enevoldsen, J.J. Eriksen, P. Ettenhuber, B. Fernández, L. Ferrighi, H. Fliegl, L. Frediani, K. Hald, A. Halkier, C. Hättig, H. Heiberg, T. Helgaker, A.C. Hennum, H. Hettema, E. Hjertenaes, S. Høst, I.-M. Høyvik, M.F. Iozzi, B. Jansík, H.J.A. Jensen, D. Jonsson, P. Jørgensen, J. Kauczor, S. Kirpekar, T. Kjaergaard, W. Klopper, S. Knecht, R. Kobayashi, H. Koch, J. Kongsted, A. Krapp, K. Kristensen, A. Ligabue, O.B. Lutnaes, J.I. Melo, K.V. Mikkelsen, R.H. Myhre, C. Neiss, C.B. Nielsen, P. Norman, J. Olsen, J.M.H. Olsen, A. Osted, M.J. Packer, F. Pawlowski, T.B. Pedersen, P.F. Provasi, S. Reine, Z. Rinkevicius, T.A. Ruden, K. Ruud, V.V. Rybkin, P. Sałek, C.C.M. Samson, A.S. de Merás, T. Saue, S.P.A. Sauer, B. Schimmelpfennig, K. Sneskov, A.H. Steindal, K.O. Sylvester-Hvid, P.R. Taylor, A.M. Teale, E.I. Tellgren, D.P. Tew, A.J. Thorvaldsen, L. Thøgersen, O. Vahtras, M.A. Watson, D.J.D. Wilson, M. Ziolkowski, H. Ågren, The Dalton quantum chemistry program system, Wiley Interdiscip. Rev. Comput. Mol. Sci. 4 (3) (2014) 269-284, https://doi.org/10.1002/wcms.1172, https:// onlinelibrary.wilev.com/doi/10.1002/wcms.1172.
- [45] J. Olsen, B.O. Roos, P. Jo/rgensen, H.J.A. Jensen, Determinant based configuration interaction algorithms for complete and restricted configuration interaction spaces, J. Chem. Phys. 89 (4) (1988) 2185–2192, https://doi.org/10.1063/1.455063, http://aip.scitation.org/doi/10.1063/1.455063.
- [46] C. Marante, L. Argenti, F. Martín, Hybrid Gaussian–B-spline basis for the electronic continuum: photoionization of atomic hydrogen, Phys. Rev. A 90 (1) (2014) 012506, https://doi.org/10.1103/PhysRevA.90.012506.
- [47] V.P. Majety, A. Scrinzi, Dynamic exchange in the strong field ionization of molecules, Phys. Rev. Lett. 115 (10) (2015) 103002, https://doi.org/10.1103/ PhysRevLett.115.103002, arXiv:1505.03349v1, http://link.aps.org/doi/10.1103/ PhysRevLett.115.103002.
- [48] V.P. Majety, A. Scrinzi, Photo-ionization of noble gases: a demonstration of hybrid coupled channels approach, Photonics 2 (1) (2015) 93–103, https://doi.org/10.3390/photonics2010093, arXiv:1412.3666, http://www.mdpi.com/2304-6732/2/1/93/.
- [49] T.N. Rescigno, D.A. Horner, F.L. Yip, C.W. McCurdy, Hybrid approach to molecular continuum processes combining Gaussian basis functions and the discrete variable representation, Phys. Rev. A 72 (2005) 052709.
- [50] F.L. Yip, C.W. McCurdy, T.N. Rescigno, Hybrid Gaussianâdiscrete-variable representation approach to molecular continuum processes: application to photoioniza-

- tion of diatomic Li_2^+ , Phys. Rev. A 78 (2) (2008) 23405, https://doi.org/10.1103/ PhysRevA.78.023405.
- [51] F.L. Yip, C.W. McCurdy, T.N. Rescigno, Hybrid Gaussianâdiscrete-variable representation for one- and two-active-electron continuum calculations in molecules, Phys. Rev. A 90 (6) (2014) 63421, https://doi.org/10.1103/PhysRevA.90.063421, http://link.aps.org/doi/10.1103/PhysRevA.90.063421.
- [52] T.-T. Nguyen-Dang, É. Couture-Bienvenue, J. Viau-Trudel, A. Sainjon, Time-dependent quantum chemistry of laser driven many-electron molecules, J. Chem. Phys. 141 (24) (2014) 244116, https://doi.org/10.1063/1.4904102, http://scitation.aip.org/content/aip/journal/jcp/141/24/10.1063/1.4904102.
- [53] F. Martín, Ionization and dissociation using B-splines: photoionization of the hydrogen molecule, J. Phys. B, At. Mol. Opt. Phys. 32 (1999) R197–R231, https://doi.org/10.1088/0953-4075/32/16/201.
- [54] H. Bachau, E. Cormier, P. Decleva, J.E. Hansen, F. Martín, Applications of B-splines in atomic and molecular physics, Rep. Prog. Phys. 64 (12) (2001) 1815–1943, https://doi.org/10.1088/0034-4885/64/12/205, http://stacks.iop.org/0034-4885/64/i=12/a=205?key=crossref.2257eec0e5040fc21410a9ef6e58af89.
- [55] P.Å. Malmqvist, B.O. Roos, B. Schimmelpfennig, The restricted active space (RAS) state interaction approach with spin–orbit coupling, Chem. Phys. Lett. 357 (3) (2002) 230–240, https://doi.org/10.1016/S0009-2614(02)00498-0.
- [56] P.G. Burke, H.M. Schey, Elastic scattering of low-energy electrons by atomic hydrogen, Phys. Rev. 126 (1) (1962) 147–162, https://doi.org/10.1103/PhysRev.126. 147.
- [57] M. Klinker, C. Marante, L. Argenti, J. González-Vázquez, F. Martín, Electron correlation in the ionization continuum of molecules: photoionization of N2 in the vicinity of the Hopfield series of autoionizing states, J. Phys. Chem. Lett. 9 (4) (2018) 756–762, https://doi.org/10.1021/acs.jpclett.7b03220.
- [58] M. Klinker, C. Marante, L. Argenti, J. González-Vázquez, F. Martín, Partial cross sections and interfering resonances in photoionization of molecular nitrogen, Phys. Rev. A 98 (3) (2018) 033413, https://doi.org/10.1103/PhysRevA.98.033413.
- [59] S.M. Poullain, M. Klinker, J. González-Vázquez, F. Martín, Resonant photoionization of O2 up to the fourth ionization threshold, Phys. Chem. Chem. Phys. 21 (2019) 16497–16504, https://doi.org/10.1039/C9CP02150G.
- [60] V.J. Borràs, J. González-Vázquez, L. Argenti, F. Martín, Molecular-frame photoelectron angular distributions of CO in the vicinity of Feshbach resonances: an XCHEM approach, J. Chem. Theory Comput. 17 (10) (2021) 6330–6339, https:// doi.org/10.1021/acs.jctc.1c00480.
- [61] P. Fernández-Milán, V.J. Borràs, J. González-Vázquez, F. Martín, Photoionization of the water molecule with XCHEM, J. Chem. Phys. 158 (13) (2023) 134305, https://doi.org/10.1063/5.0139738.
- [62] L. Barreau, C.L.M. Petersson, M. Klinker, A. Camper, C. Marante, T. Gorman, D. Kiesewetter, L. Argenti, P. Agostini, J. González-Vázquez, P. Salières, L.F. DiMauro, F. Martín, Disentangling spectral phases of interfering autoionizing states from attosecond interferometric measurements, Phys. Rev. Lett. 122 (25) (2019) 253203, https://doi.org/10.1103/PhysRevLett.122.253203.
- [63] R.Y. Bello, V.J. Borràs, J. González-Vázquez, F. Martín, Electronic coherences in argon through interfering one- and two-photon ionization processes in the vicinity of Feshbach resonances, Phys. Rev. Res. 4 (4) (2022) 043028, https://doi.org/10. 1103/PhysRevResearch.4.043028.
- [64] V.J. Borràs, J. González-Vázquez, L. Argenti, F. Martín, Attosecond photoionization delays in the vicinity of molecular Feshbach resonances, Sci. Adv. 9 (15) (2023) eade3855, https://doi.org/10.1126/sciadv.ade3855.
- [65] C. Marante, M. Klinker, T. Kjellsson, E. Lindroth, J. González-Vázquez, L. Argenti, F. Martín, Photoionization using the xchem approach: total and partial cross sections of Ne and resonance parameters above the \$2{s}{2}2{p}{5}\$ threshold, Phys. Rev. A 96 (2) (2017) 022507, https://doi.org/10.1103/PhysRevA.96.022507.
- [66] The HDF Group, Hierarchical data format, version 5, https://www.hdfgroup.org/ HDF5/ (1997-2023).

- [67] N. Harkema, C. Cariker, E. Lindroth, L. Argenti, A. Sandhu, Autoionizing polaritons in attosecond atomic ionization, Phys. Rev. Lett. 127 (2021) 023202, https://doi.org/10.1103/PhysRevLett.127.023202, https://link.aps.org/doi/10.1103/PhysRevLett.127.023202.
- [68] R.G. Newton, Scattering Theory of Waves and Particles, Springer Science & Business Media, 2013.
- [69] A. Rouzée, F. Kelkensberg, W. Kiu Siu, G. Gademann, R.R. Lucchese, M.J.J. Vrakking, J. Phys. B, At. Mol. Phys. 45 (2012) 074016, https://doi.org/10.1088/0953-4075/45/7/074016, http://adsabs.harvard.edu/abs/2012JPhB...45g4016R.
- [70] P.M. Dehmer, P.J. Miller, W.A. Chupka, Photoionization of N2 X1Σ+g, v"=0 and 1 near threshold. Preionization of the Worley–Jenkins Rydberg series, J. Chem. Phys. 80 (3) (1984) 1030–1038, https://doi.org/10.1063/1.446829.
- [71] W.B. Peatman, B. Gotchev, P. Gürtler, E.E. Koch, V. Saile, Transition probabilities at threshold for the photoionization of molecular nitrogen, J. Chem. Phys. 69 (5) (1978) 2089–2095, https://doi.org/10.1063/1.436808.
- [72] K.P. Huber, G. Stark, K. Ito, Rotational structure in the Hopfield series of N2, J. Chem. Phys. 98 (6) (1993) 4471–4477, https://doi.org/10.1063/1.465006.
- [73] P. Gürtler, V. Saile, E.E. Koch, High resolution absorption spectrum of nitrogen in the vacuum ultraviolet, Chem. Phys. Lett. 48 (2) (1977) 245–250, https://doi.org/10.1016/0009-2614(77)80308-4, https://www.sciencedirect.com/science/ article/pii/0009261477803084.
- [74] J.B. West, K. Codling, A.C. Parr, D.L. Ederer, B.E. Cole, R. Stockbauer, J.L. Dehmer, Branching ratios and photoelectron angular distributions through the Hopfield bands in N2 between 650 and 730 AA, J. Phys. B, At. Mol. Phys. 14 (11) (1981) 1791, https://doi.org/10.1088/0022-3700/14/11/015.
- [75] P. Fernández-Milán, V.J. Borràs, J. González-Vázquez, F. Martín, Photoionization of the water molecule with XCHEM, J. Chem. Phys. 158 (13) (04 2023) 134305, https://doi.org/10.1063/5.0139738, https://pubs.aip.org/aip/jcp/article-pdf/doi/ 10.1063/5.0139738/16823439/134305_1_5.0139738.pdf.
- [76] C. Winstead, V. McKoy, Low-energy electron scattering by pyrazine, Phys. Rev. A 76 (1) (2007) 012712, https://doi.org/10.1103/PhysRevA.76.012712, https://link.aps.org/doi/10.1103/PhysRevA.76.012712.
- [77] C. Winstead, V. McKoy, Resonant channel coupling in electron scattering by pyrazine, Phys. Rev. Lett. 98 (11) (2007) 113201, https://doi.org/10.1103/PhysRevLett.98.113201, https://link.aps.org/doi/10.1103/PhysRevLett.98.113201.
- [78] C. Fridh, L. Åsbrink, B. Jonsson, E. Lindholm, XV. Photoelectron, mass and electron impact spectra of pyrazine, Int. J. Mass Spectrom. Ion Phys. 8 (2) (1979) 101–118, https://doi.org/10.1016/0020-7381(72)80002-0, https://www.sciencedirect.com/science/article/pii/0020738172800020.
- [79] R. Scheps, D. Florida, S.A. Rice, Comments on the Rydberg spectrum of pyrazine, J. Mol. Spectrosc. 44 (1) (1972) 1–13, https://doi.org/10.1016/0022-2852(72)90188-9. https://www.sciencedirect.com/science/article/pii/0022285272901889.
- [80] M.N. Piancastelli, P.R. Keller, J.W. Taylor, Angular distribution parameter as a function of photon energy for some mono- and diazabenzenes and its use for orbital assignment, J. Am. Chem. Soc. 105 (13) (1983) 4235–4239, https://doi.org/10.1021/ja00351a019, http://pubs.acs.org/doi/abs/10.1021/ja00351a019.
- [81] Y.-i. Suzuki, T. Suzuki, Photoelectron angular distribution in valence shell ionization of heteroaromatic molecules studied by the continuum multiple scattering Xα method, J. Phys. Chem. A 112 (3) (2008) 402–411, https://doi.org/10.1021/jp077064h.
- [82] D. Holland, A. Potts, L. Karlsson, M. Stener, P. Decleva, A study of the valence shell photoionisation dynamics of pyrimidine and pyrazine, Chem. Phys. 390 (1) (2011) 25–35, https://doi.org/10.1016/j.chemphys.2011.09.025, https://www.sciencedirect.com/science/article/pii/S0301010411004186.